Carrier dynamics of silicon vacancies of SiC under simultaneous optically and electrically excitations

View Online   Export Citation   CrossMark

Yuichi Yamazaki,[1,a] Yoji Chiba,[1,2] Shin-ichiro Sato,[1] Takahiro Makino,[1] Naoto Yamada,[1] Takahiro Satoh,[1] Kazutoshi Kojima,[3] Yasuto Hijikata,[2] Hidekazu Tsuchida,[4] Norihiro Hoshino,[4] Sang-Yun Lee,[5] and Takeshi Ohshima[1]

AFFILIATIONS

[1] National Institutes for Quantum and Radiological Science and Technology (QST), Takasaki, Gunma 370-1292, Japan
[2] Graduate School of Science and Engineering, Saitama University, Saitama 338-8570, Japan
[3] National Institute of Advanced Industrial Science and Technology, Tsukuba, Ibaraki 305-8568, Japan
[4] Central Research Institute of Electric Power Industry, Yokosuka, Kanagawa 240-0196, Japan
[5] Department of Physics and Photon Science at Gwangju Institute of Science and Technology, Gwangju 123, South Korea

[a] Author to whom correspondence should be addressed: yamazaki.yuichi@qst.go.jp

ABSTRACT

Silicon carbide (SiC) is an important wide bandgap semiconductor used for diverse applications from heat spreading to high-power electronics. It is readily doped, has high thermal conductivity, and is used for application in mature device fabrication techniques. To improve the performance of SiC electronic devices, built-in sensors, which should ideally be inexpensive integrated with the device, and not perturb device operations, are quite useful. Here, we studied the optical properties of the negatively silicon vacancy under simultaneous optical and electrical excitation to uncover the carrier dynamics, as the luminescence intensity is determined by competition between the two excitation pathways. We also observe optically detected magnetic resonance (ODMR) and observe that the ODMR contrast is decreased by injected current, which is consistent with the decrease in the pumping rate of optical excitation in the competitive process. Our studies show that an embedded quantum sensor is possible in practical SiC devices, opening new opportunities for device control and optimization.

Silicon carbide (SiC) is one of the most commercially important semiconductor materials and continues to have a growing impact on global science and technology.[1] As a wide bandgap semiconductor with mature lithographic and doping techniques, it finds applications as diverse as high-efficiency electronics, automotive parts, and high-power electronics.

With the continuous development of SiC devices, it becomes increasingly important to monitor device properties in real time.[2,3] This can be important for improving efficiency, failure prediction, and device simulation. Ideally, one would like low-cost, embedded sensor solutions, with remote monitoring, capable of operation in the current and temperature ranges of SiC devices (for reference values, 1–10 A and 20–200 °C, respectively), which will not perturb device operation. It is likely that no single sensor solution will meet all the sensor requirements for all the diverse applications of SiC. Nevertheless, some of the embedded defects in SiC, including the negatively silicon vacancy (V_{Si}^-)[4,5] and the neutral divacancy (V_C–V_{Si}, VV^0),[6,7] hold promise for quantum sensing solutions. Specifically, a V_{Si}^--based quantum sensor is possible to detect the magnetic field and

temperature with high sensitivity and spatial resolution at room temperature.[8,9] In principle, these quantities can be measured simultaneously to realize a single multi-modality sensor.

Quantum sensing using embedded defects uses optically detected magnetic resonance (ODMR), where physical quantities are sensed by analyzing the change in emission intensity from optically excited spin defects. Because we are interested in realistic device performance, we performed these measurements under various electrical bias and current conditions. Although there have been previous studies performed under electrical bias for charge state control of spin defects[7,10] and Stark-shift tuning of the optical transition frequencies,[7,11] these studies did not observe electroluminescence (EL) as they were operated under reverse bias and the device structure was not designed for EL. Hence, to date, the change in optical properties of spin defects caused by EL has not been treated. As mentioned above, practical devices are likely to be operated under both forward and reverse bias, and under forward bias, EL is not negligible. Although EL of V_{Si}^- has been discussed,[10,12] it is not enough to consider solely the change in optical properties of V_{Si}^-. It is necessary to understand carrier dynamics of

V_{Si}^- under simultaneous optical and electrical excitations to understand how this defect operates as a practical quantum sensor of a working device.

Here, we show the optical properties of V_{Si}^- under simultaneous optical and electrical excitation to understand the carrier dynamics and the effect of electroexcitation (EE) on photoexcitation (PE). We fabricated pn junction diodes to limit the current path and created a three-dimensional array of V_{Si}^- distributed in and out of the current path.[13] In addition, we show that ODMR measurements of a device with applied current are possible using adjusted measurement conditions from those used for optimal photoluminescence (PL).

A cross-sectional view of the sample is shown in Fig. 1(a). The junctions were created on 5.6-μm-thick p-type epitaxial layers with a doping concentration of 1.5×10^{16} cm^{-3} on an n-type substrate (see supplementary material Sec. 1 for diode characteristics and related

discussions). For current injection (both electrons and holes) into the epitaxial layer, the p$^+$- and n$^+$-type regions were independently formed by aluminum (a concentration of 2×10^{20} cm^{-3}) and phosphorus (concentration of 5×10^{19} cm^{-3}) ion implantations, respectively, at 800 °C. Annealing was subsequently performed at 1800 °C for 5 min in an argon atmosphere for dopant activation. Then, aluminum was deposited onto the p$^+$- and n$^+$-type regions to form metal electrodes.

The three-dimensional array of V_{Si}^- was introduced in close proximity to the two electrodes by particle beam writing (PBW)[14] using a focused ($\sim$1 μm) He beam and a dot pattern with a pitch of 10 μm in which the electrodes are used as landmarks, with a fluence of 1×10^6 He$^+$/spot. Note that annealing at more than 700 °C leads to the disappearance of V_{Si}^-, which is why the PBW step is performed after diode fabrication.[5] We used ion energies of 0.5, 1.5, and 3 MeV to vary the
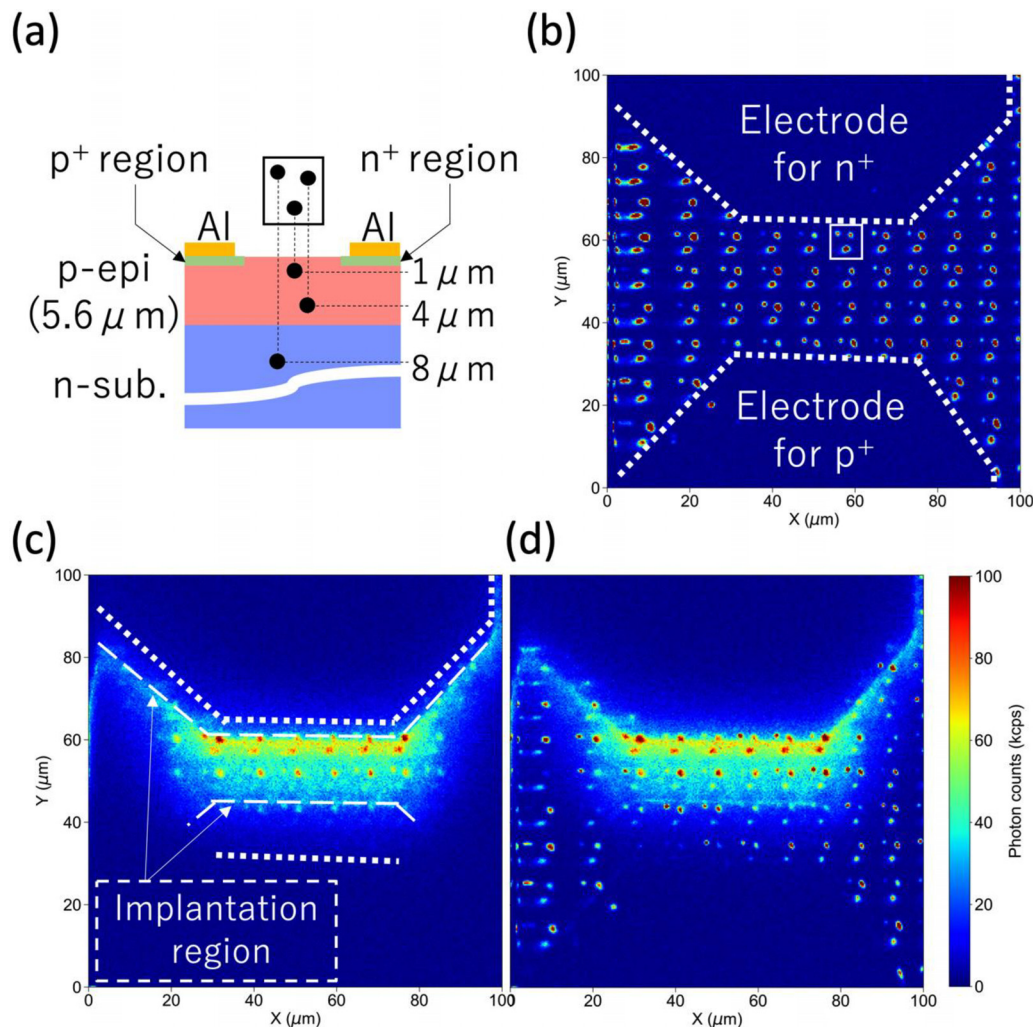

FIG. 1. A cross-sectional view of the sample (a) and luminescence intensity mappings of the sample irradiated with 1×10^6 (0.5, 1.5, and 3 MeV) upon (b) PE (100 μW), (c) EE (3 mA), and (d) simultaneous excitation (100 μW + 3 mA). The color bar in (d) is common for (b)–(d). A cluster of three different luminescent spots is boxed with a white square in (b). The boundaries of electrodes and implantation regions are depicted by white dotted lines in (b) and (c). The asymmetry between the electrode and the implantation region shown in (c) was caused by the misalignment during photolithography.

depth of V_{Si}^-, which gives depths of $\sim$1, 4, and 8 μm, respectively, as estimated using SRIM.[15] To easily distinguish these depths optically, the sample position was slightly shifted between irradiations. Samples were then annealed at 400 °C to improve the optical properties of V_{Si}^- and avoid degradation of the Al electrodes although 600 °C is the best temperature for improving the optical properties of V_{Si}^-.[16]

A home-built confocal microscope (CFM) was used to investigate optical properties. A 671 nm laser and a forward current of the pn junction were utilized for PE and EE, respectively. For ODMR measurements, the RF excitation excited the sample via a copper coil (33 dBm) positioned just behind the backside of the sample. 830 nm and 900 nm long-pass filters were used to remove background luminescence.

Figures 1(b)–1(d) show the luminescence intensity mappings upon (b) PE (100 μW), (c) EE (3 mA), and (d) simultaneous excitation. Under PE, the luminescent dot array showing the three different implantation energies is clearly observed throughout the area except under the two electrodes. We can confirm the implantation depth by changing the focal point of the CFM and find the top-left, top-right, and bottom spots located deepest ($\sim$8 μm), shallowest ($\sim$1 μm), and middle ($\sim$4 μm), respectively. For EE, luminescent spots were observed only in the vicinity of two electrodes. Broadly distributed luminescence between two electrodes shown in Fig. 1(c) is attributed to other defects introduced by PBW. A similar luminescence was observed in the case of EE.[17,18]

To investigate luminescence intensity under simultaneous excitation in more detail, the excitation intensity dependence of luminescence intensity was studied. Figure 2 shows luminescence intensity as a function of injected current into the p-type epitaxial layer upon various laser powers from the (a) middle and (b) deepest spots, positioned at the center of the electrode and the closest to the electrode for the n^+ region [boxed with a white square in Fig. 1(a)]. The intensity was decreased by small current injection for all laser power conditions. Upon further increasing the current, it became almost constant for higher laser powers ($>$100 μW), whereas it increased for lower laser powers. In contrast, no significant change was observed in the case of the deepest spot. It is noted that current was not injected into the deepest spot due to a

depletion region at the interface between the epitaxial layer and the substrate. A comparison of these results suggests that the current is responsible for the change in the intensity observed for the middle spot.

The fundamental processes of PE and EE at V_{Si}^- can be considered as follows. In the PE process, an electron in V_{Si}^- [ground state (GS)] can be excited to V_{Si}^- [excited state (ES)]. On the other hand, previous reports suggest that the EE process for electron excitation of V_{Si}^- is via a hole and subsequent electron capture via a neutral state of V_{Si} (V_{Si}^0).[10,12] Finally, PL and EL are emitted via direct transition from the ES to the GS for PE and EE, respectively, which is supported by the experimental result that the EL spectrum was similar to that of PL.[17,18] Electrons in V_{Si}^- (ES) show a nonradiative transition via a shelving state rather than direct transition with a certain probability. The fundamental processes of PE and EE and all transitions under simultaneous excitation are summarized in Figs. 3(a)–3(c), respectively, where $|1\rangle \sim |4\rangle$ denote V_{Si}^- (GS), V_{Si}^- (ES), shelving state, and V_{Si}^0, respectively, and the corresponding pumping and transition rates are denoted by k_{ij}. This figure indicates that PE and EE processes are in competition under simultaneous excitation.

We analyzed the change in luminescence intensity under simultaneous excitation quantitatively using rate equations to reveal how this competition affects the intensity, especially PL. The values of k_{12} and k_{14} cannot be used for the analysis of the results under simultaneous excitation due to competitive processes. In this case, these should be adjusted on a weighted average. Using weighted average pumping rates (k^*_{12} and k^*_{14}) obtained from a conversion formula, $k^*_{ij} = k_{ij}^2/(k_{12} + k_{14})$, the rate equations under simultaneous excitation are expressed as follows:

$$\frac{dp_1}{dt} = -k^*_{12} \cdot p_1 - k^*_{14} \cdot p_1 + k_{21} \cdot p_2 + k_{31} \cdot p_3,$$

$$\frac{dp_2}{dt} = k^*_{12} \cdot p_1 + k^*_{42} \cdot p_4 - k_{21} \cdot p_2 - k_{23} \cdot p_2,$$

$$\frac{dp_3}{dt} = k_{23} \cdot p_2 - k_{31} \cdot p_3,$$

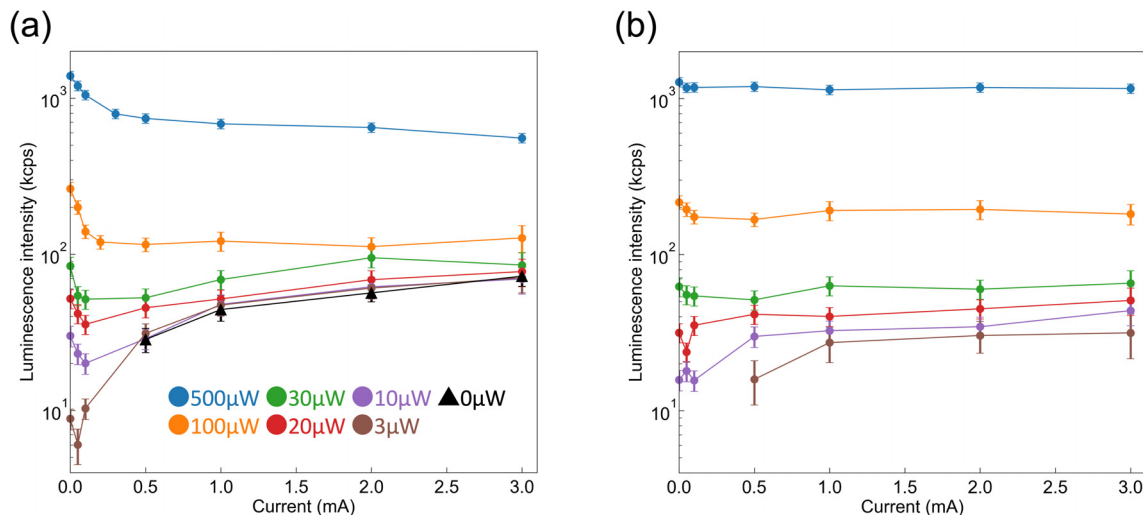$$\frac{dp_4}{dt} = k^*_{41} \cdot p_1 - k^*_{42} \cdot p_4,$$

FIG. 2. Luminescence intensity as a function of injected current at various laser powers from the (a) middle and (b) deepest spots. A different trend was obtained between (no) current injected in the middle (deepest) spots.
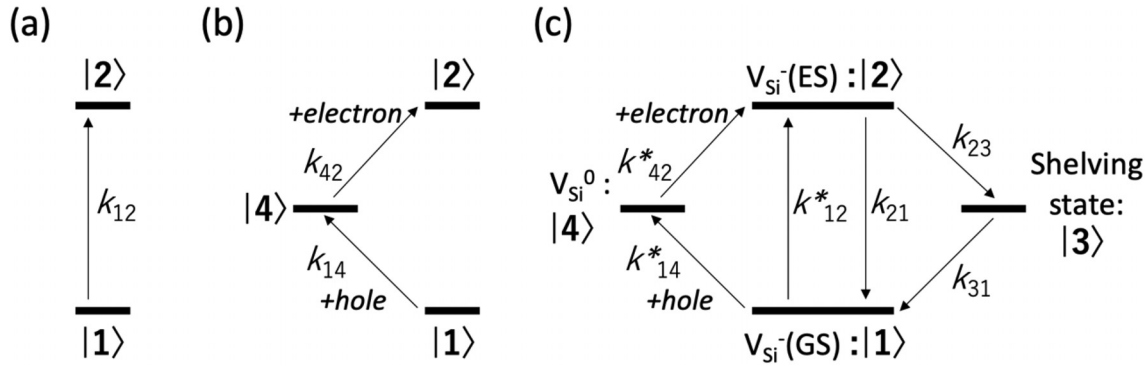
FIG. 3. The fundamental processes of (a) PE and (b) EE and (c) all transitions under simultaneous excitation for V_{Si}^-. The states $|1\rangle \sim |4\rangle$ denote V_{Si}^- (GS), V_{Si}^- (ES), shelving state, and V_{Si}^0. The corresponding pumping and transition rates are also denoted by k_{ij}.

where p_1–p_4 are the population of states $|1\rangle \sim |4\rangle$. k_{12} and k_{14} can be determined by analyzing the experimental results of PE [PL for 0 mA in Fig. 2(a)] and EE [EL in Fig. 2(a)] using the rate equations for k_{14} = 0 or k_{12} = 0, respectively. Figure 4 shows calculated k_{12} and k_{14} as a function of laser power and current, respectively (see supplementary material Sec. 2 for the results in the case of other fluences in PBW). A set of k_{14} in the range of 0.01–0.1 mA was determined from the extrapolation of the dotted lines. Following Hain et al.,[19] the transition rate k_{21} was set to be 1/6 ns^{-1}. In the T_1 measurement using V_{Si}^-,[4] the laser pulse width was set to 400 ns, which means that a transition time via the shelving state ($1/k_{23} + 1/k_{31}$) is estimated to be at least 400 ns or less. Therefore, k_{23} and k_{31} were assumed to be 1/100 ns^{-1} in this work, respectively. Average excitation times, $1/k^*_{12}$ and $1/k^*_{14}$, were much longer than 100 ns. We confirmed that increasing or decreasing $1/k_{23}$ and $1/k_{31}$ by one order of magnitude from the order of 100 ns

did not change our conclusion. Although k_{42} is also required for the analysis, we could not determine it experimentally in this work. From the fundamental processes of EE, it is found that k_{14} and k_{42} are roughly proportional to the number of holes and electrons, and $k_{42} \gg k_{14}$ is expected from doping concentrations. We varied the ratio between k^*_{14} and k^*_{42} until we obtained the best fit for the data obtained under simultaneous excitation. Such fitting leads us to conclude that $k^*_{42} = 300 \times k^*_{14}$. This value is larger than the doping concentration difference, and we speculate that k^*_{14} may be enhanced by the Coulomb force between V_{Si}^- and h$^+$.[20]

Using these pumping and transition rates and initial conditions, $p_1 = 1$ and $p_2 = p_3 = p_4 = 0$ at t = 0, we analyzed luminescence intensity under simultaneous excitation. Luminescence intensity is calculated from $1 \times 10^9 \times k_{21} \times p_2 \times N_{VSi}$ (counts per second), where N_{VSi} is the number of V_{Si}^- in a spot. From the reported V_{Si}^- creation yield ~ 0.1 per H$^+$[14] and the result of SRIM simulation that He$^+$ ions generate eight times more vacancies than H$^+$ ions in SiC,[15] we estimate that $N_{VSi} = 8 \times 10^5$/spot for a fluence of 1×10^6 (see supplementary material Sec. 3 for the detailed discussions). Experimental and simulated luminescence intensities are shown in Fig. 5. The inset schematically represents the value of k_{12} and k_{14} by the thickness of the arrows for (i) high and (ii) low laser powers. The simulated intensities were in good agreement with the experimental ones. The luminescence intensity decreases for all laser power conditions for small current because the pumping rate for PE decreases by current injection (k_{12} to k^*_{12}). A similar ratio of k_{12} to k_{14} leads to no remarkable change in luminescence intensity upon further increasing the current at high laser powers. In contrast, at low laser powers, since EE is more dominant, the luminescence intensity shows a decreasing to increasing trend with increasing current, which is attributed to the increase in EL.

Finally, we checked the effect of EE against ODMR contrast under simultaneous excitation (100 and 500 μW, 0–3 mA) using the shallowest spot. The ODMR contrast is given by ΔPL/(PL + EL) under simultaneous optical and electrical excitation, where ΔPL is the increase in PL intensity in resonance. In EE, it is assumed that there is no spin polarization, resulting in ΔEL = 0. Only electrons absorbing electromagnetic waves (resonance) (process 1) followed by PE (process 2) can contribute to the ΔPL. Competition between PE and EE occurs in each process of 1 and 2, which means that the numerator is decreased by a factor of c^2 [$c = k_{12}/(k_{12} + k_{14})$]. On the other hand,
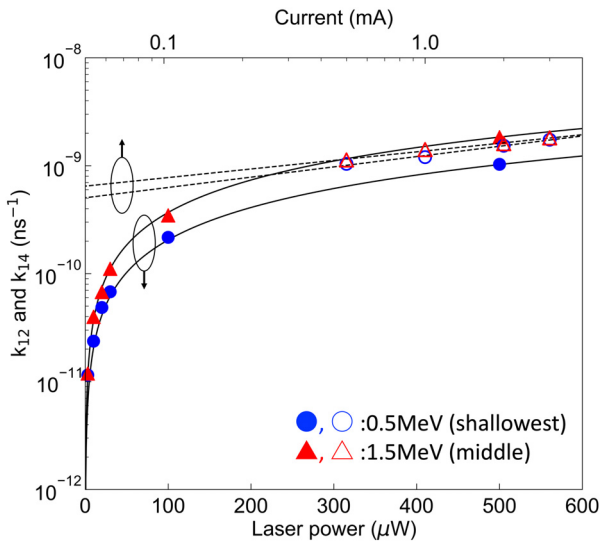

FIG. 4. Calculated k_{12} (closed symbol) and k_{14} (open symbol) under PE and EE, respectively, for the shallowest and middle spots. When analyzing k_{14}, k_{42} was set to be $300 \times k_{14}$ (the calculation method is described in the text). The solid lines for k_{12} are the result of linear fitting. The dotted lines for k_{14} are extrapolated lines.
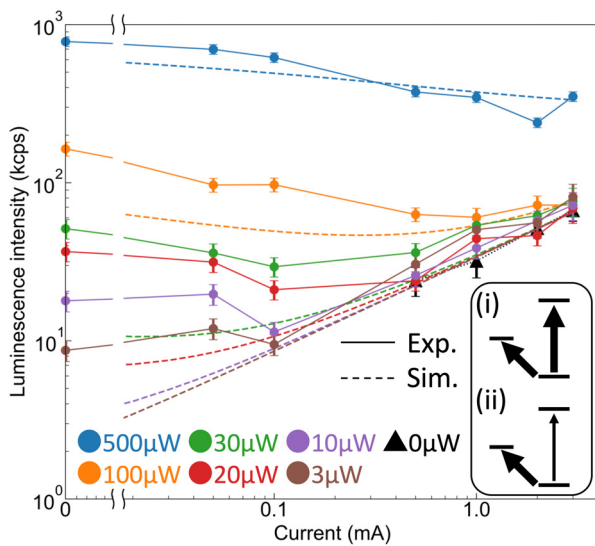
FIG. 5. Experimental (solid symbols and lines) and simulated (dotted lines) luminescence intensities as a function of injected current at various photoexcitation powers for the shallowest spot. The inset schematically represents the values of k_{12} and k_{14} by the thickness of the arrows for (i) high and (ii) low laser powers.

the denominator decreases by a factor of c. Therefore, the contrast is roughly reduced by a factor of c (the denominator EL is negligible if PL ≫ EL). Figure 6 shows normalized k^*_{12} ($= c$) and ODMR contrast as a function of current. The ODMR contrast abruptly decreased in the low current region and then gradually decreased. The normalized k^*_{12} was found to decrease in a similar manner. Based on these results, the ODMR contrast under simultaneous excitation can be explained by a decrease in the pumping rate of PE.
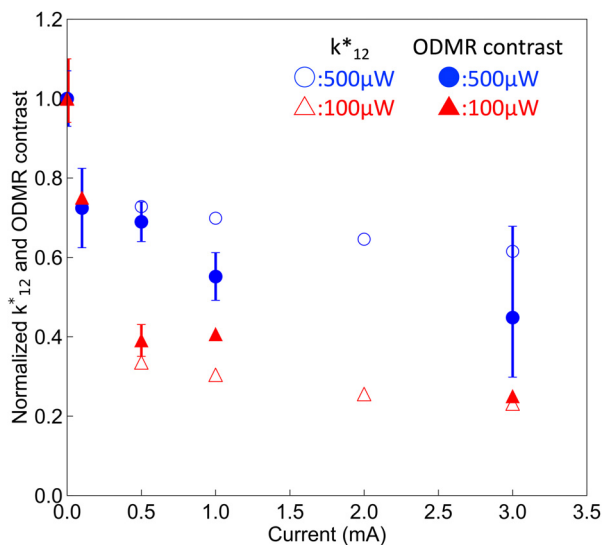

FIG. 6. Normalized k^*_{12} and ODMR contrast as a function of current for 100 and 500 μW for the shallowest spot.

In summary, we investigated optical properties of V_{Si}^- under simultaneous optical and electrical excitation to elucidate carrier dynamics and explore the possibility of ODMR sensing of a working device under forward bias. The PE and EE pathways compete under simultaneous excitation, which modifies the effective pumping rates that are observed. This combination leads to either an increase or decrease in luminescence intensity with increasing current depending on a laser power. The ODMR contrast decreased with increasing current, which was caused by the decrease in the pumping rate of PE. A numerical simulation based on the rate equations using weighted average pumping rates was in good agreement with experimental data under simultaneous excitation. The carrier dynamics of V_{Si}^- revealed in this work clearly shows that the inside of the SiC device during operation can be observed using a V_{Si}^--based quantum sensor with appropriate conditions, leading to a minimal amount of PL to obtain the ODMR spectrum even if a large amount of current is applied. In addition, a sensitive change in luminescence intensity caused by a balance of pumping rates of PE and EE is applicable to a simplified current monitor to obtain current distribution. The analysis method used in this study will provide insight into both the energy-level diagram and the carrier dynamics for other spin defects.

See the supplementary material for (1) diode characteristics and the influence of applied voltages on the optical properties of V_{Si}^-, (2) pumping rates of PE and EE as a function of fluence in PBW, and (3) estimation of the number of V_{Si}^-.

DATA AVAILABILITY

The data that support the findings of this study are available within this article and its supplementary material.

REFERENCES

[1]X. She, A. Q. Huang, Ó. Lucía, and B. Ozpineci, IEEE Trans. Ind. Electron. **64**, 8193 (2017).
[2]A. Griffo, J. Wang, K. Colombage, and T. Kamel, IEEE Trans. Ind. Electron. **65**, 2663 (2018).
[3]F. Erturk, E. Ugur, J. Olson, and B. Akin, IEEE Trans. Ind. Electron. **55**, 600 (2019).
[4]M. Widmann, S.-Y. Lee, T. Rendler, N. T. Son, H. Fedder, S. Paik, L.-P. Yang, N. Zhao, S. Yang, I. Booker, A. Denisenko, M. Jamali, S. A. Momenzadeh, I. Gerhardt, T. Ohshima, A. Gali, E. Janzén, and J. Wrachtrup, Nat. Mater. **14**, 164 (2015).
[5]F. Fuchs, B. Stender, M. Trupke, D. Simin, J. Pflaum, V. Dyakonov, and G. V. Astakhov, Nat. Commun. **6**, 7578 (2015).
[6]D. J. Christle, A. L. Falk, P. Andrich, P. V. Klimov, J. Ul Hassan, N. T. Son, E. Janzén, T. Ohshima, and D. D. Awschalom, Nat. Mater. **14**, 160 (2015).
[7]C. F. de las Casas, D. J. Christle, J. U. Hassan, T. Ohshima, N. T. Son, and D. D. Awschalom, Appl. Phys. Lett. **111**, 262403 (2017).
[8]S. A. Tarasenko, A. V. Poshakinskiy, D. Simin, V. A. Soltamov, E. N. Mokhov, P. G. Baranov, V. Dyakonov, and G. V. Astakhov, Phys. Status Solidi B **255**, 1700258 (2018).
[9]T. Ohshima, T. Satoh, H. Kraus, G. V. Astakhov, V. Dyakonov, and P. G. Baranov, J. Phys. D **51**, 333002 (2018).

[10] M. Widmann, M. Niethammer, D. Y. Fedyanin, I. A. Khramtsov, T. Rendler, I. D. Booker, J. Ul Hassan, N. Morioka, Y.-C. Chen, I. G. Ivanov, N. T. Son, T. Ohshima, M. Bockstedte, A. Gali, C. Bonato, S.-Y. Lee, and J. Wrachtrup, Nano Lett. **19**, 7173 (2019).

[11] C. P. Anderson, A. Bourassa, K. C. Miao, G. Wolfowicz, P. J. Mintun, A. L. Crook, H. Abe, J. Ul Hassan, N. T. Son, T. Ohshima, and D. D. Awschalom, Science **366**, 1225 (2019).

[12] G. Wolfowicz, C. P. Anderson, A. L. Yeats, S. J. Whiteley, J. Niklas, O. G. Poluektov, F. J. Heremans, and D. D. Awschalom, Nat. Commun. **8**, 1876 (2017).

[13] Y. Yamazaki, Y. Chiba, S.-I. Sato, T. Makino, N. Yamada, T. Satoh, K. Kojima, Y. Hijikata, H. Tsuchida, N. Hoshino, S.-Y. Lee, and T. Ohshima, Mater. Sci. Forum **1004**, 343 (2020).

[14] H. Kraus, D. Simin, C. Kasper, Y. Suda, S. Kawabata, W. Kada, T. Honda, Y. Hijikata, T. Ohshima, V. Dyakonov, and G. V. Astakhov, Nano Lett. **17**, 2865 (2017).

[15] See http://www.srim.org/ for "SRIM: The Stopping and Range of Ions in Matter."

[16] Y. Chiba, Y. Yamazaki, S.-I. Sato, T. Makino, N. Yamada, T. Satoh, Y. Hijikata, and T. Ohshima, Mater. Sci. Forum **1004**, 337 (2020).

[17] Y. Yamazaki, Y. Chiba, T. Makino, S.-I. Sato, N. Yamada, T. Satoh, Y. Hijikata, K. Kojima, S.-Y. Lee, and T. Ohshima, J. Mater. Res. **33**, 3355 (2018).

[18] F. Fuchs, V. A. Soltamov, S. Väth, P. G. Baranov, E. N. Mokhov, G. V. Astakhov, and V. Dyakonov, Sci. Rep. **3**, 1637 (2013).

[19] T. C. Hain, F. Fuchs, V. A. Soltamov, P. G. Baranov, G. V. Astakhov, T. Hertel, and V. Dyakonov, J. Appl. Phys. **115**, 133508 (2014).

[20] I. A. Khramtsov, A. A. Vyshnevyy, and D. Yu. Fedyanin, npj Quantum Inf. **4**, 15 (2018).